Time-Resolved UV Resonance Raman Investigation of Protein Folding Using a Rapid Mixer: Characterization of Kinetic Folding Intermediates of Apomyoglobin†

Nami Haruta‡ and Teizo Kitagawa*,‡,§

School of Mathematical and Physical Sciences, The Graduate University for Advanced Studies, Myodaiji, Okazaki 444-8585, Japan, and Center for Integrative Bioscience, Okazaki National Research Institutes, Myodaiji, Okazaki 444-8585, Japan

Received November 6, 2001

ABSTRACT: The 244-nm excited transient UV resonance Raman spectra are observed for the refolding intermediates of horse apomyoglobin (h-apoMb) with a newly constructed mixed flow cell system, and the results are interpreted on the basis of the spectra observed for the equilibrium acid unfolding of the same protein. The dead time of mixing, which was determined with the appearance of UV Raman bands of imidazolium upon mixing of imidazole with acid, was 150 μs under the flow rate that was adopted. The pH-jump experiments of h-apoMb from pH 2.2 to 5.6 conducted with this device demonstrated the presence of three folding intermediates. On the basis of the analysis of W3 and W7 bands of Trp7 and Trp14, the first intermediate, formed before 250 μs, involved incorporation of Trp14 into the α-helix from a random coil. The frequency shift of the W3 band of Trp14 observed for this process was reproduced with a model peptide of the A helix when it forms the α-helix. In the second intermediate, formed around 1 ms after the start of refolding, the surroundings of both Trp7 and Trp14 were significantly hydrophobic, suggesting the formation of the hydrophobic core. In the third intermediate appearing around 3 ms, the hydrophobicity was relaxed to the same level as that of the pH 4 equilibrium intermediate, which was investigated in detail with the stationary state technique. The change from the third intermediate to the native state needs more time than 40 ms, while the appearance of the native spectrum after the mixing of the same solutions was confirmed separately.

Since Anfinsen's finding of the principal dogma about a protein structure (*1*), understanding the tertiary structure formation on the basis of a primary structure has become an attractive subject of fundamental chemistry, and computer formation of a folded protein from random structures based on the first principle is becoming realistic (*2*, *3*), although the size of the polypeptides is currently limited. On the other hand, all the newly developed experimental techniques which may possibly elucidate the folding process have been applied to promote the current understanding of its mechanism, particularly in the structural embodiment of the free energy funnel (*4*). Since protein folding is a generally cooperative process, the buildup of folding intermediates hardly takes place, and therefore, spectroscopic identification of intermediates requires time-resolved experiments. During this process, interactions among side chains of individual amino acid residues as well as that in a peptide backbone play important roles, because proteins with different sequences fold into different structures. Time-resolved IR spectroscopy can provide information about the main chain structures through amide I and II bands with high time resolution (*5*). Fluorescence spectroscopy in its application to the folding problem suggests that fluorescence intensity reflects a distance between an emitter (aromatic side chains) and a quencher. With other available techniques, it is generally difficult to obtain specific information about the side chain arrangements and their environments for the events occurring on a time scale faster than milliseconds.

Resonance Raman spectroscopy is a technique for observing the vibrational spectra of chromophores selectively and sensitively by tuning a Raman excitation wavelength to an absorption maximum of the chromophore of molecules (*6*), and has been extensively used to explore ultrafast dynamics of proteins (*7*) as well as structural analysis of stationary states and reaction intermediates (*8*). Because of recent technical developments of UV lasers, ultraviolet resonance Raman spectroscopy (UVRR)[1] increasingly attracts general attention as a powerful tool for detection of protein conformational changes (*9*) and is indeed used to characterize conformational changes of proteins, particularly of hemo-

† This study was supported by a Grant-in-Aid for Scientific Research from the Ministry of Education, Science, Sports and Culture, Japan, to T.K. (13308039).

* To whom correspondence should be addressed. Telephone: +81-564-59-5225. Fax: +81-564-59-5229. E-mail: teizo@ims.ac.jp.

‡ The Graduate University for Advanced Studies.

§ Okazaki National Research Institutes.

[1] Abbreviations: UVRR, ultraviolet resonance Raman; Mb, myoglobin; apoMb and holoMb, apomyoglobin and holomyoglobin, respectively; hMb and swMb, horse Mb and sperm whale Mb, respectively; h-apoMb and sw-apoMb, horse and sperm whale apoMb, respectively; IR, infrared; NMR, nuclear magnetic resonance; CD, circular dichroism; NOE, nuclear Overhauser effect; A peptide, model peptide of the A helix region of Mb; HPLC, high-performance liquid chromatography; Tris, tris(hydroxymethyl)aminomethane; CW, continuous wave; Im and ImH^+, imidazole and imidazolium, respectively; N, native; I, intermediate; U, unfolded; TFE, 2,2,2-trifluoroethanol; MeOH, methanol.

10.1021/bi012027g CCC: $22.00
Published on Web 05/03/2002

globin (*10*−*13*). Indeed, this technique was applied to the protein folding problems by Copeland and Spiro for cytochrome *c* (*14*) and by Chi and Asher, who used 229 and 206.5 nm excitation for analysis of horse holoMb (*15*) and apoMb (h-apoMb) (*16*), demonstrating the promising prospect of the technique. More recently, Lednev et al. (*17*) applied it to explore the fast dynamics of α-helical alanine-rich polypeptides, and Hashimoto et al. (*18*) investigated acid-unfolded intermediates of sperm whale apoMb (sw-apoMb). However, there have been no kinetic UVRR studies of protein folding from the almost completely unfolded state. Accordingly, we have constructed the rapid mixing device reported by Takahashi et al. (*19*) and combined it with time-resolved UVRR spectroscopy to explore the primary process in folding of apoMb.

The folding and unfolding intermediates of apoMb have been investigated with various techniques, including NMR (*20*−*22*), CD (*23*−*25*), fluorescence (*26*, *27*), small-angle X-ray scattering (*28*, *29*), IR (*5*, *30*), and UVRR techniques (*15*, *16*, *18*). Mb has eight helices, labeled A−H, and a heme is connected to the globin with a covalent bond via His93 of the F helix. ApoMb has seven helices as a result of melting of the F helix upon removal of the heme (*31*, *32*) and is known to give a stable acid unfolding intermediate at pH 4 (*20*), which has been considered to be the same as a kinetic intermediate in the refolding process (*21*). This intermediate contains helices A, B, G, and H with the nativelike contacts, called the AGH hydrophobic core. Previously, we have characterized the UVRR spectra of Trp7 and Trp14 separately using W14F and W7F mutants of Mb, respectively, and pointed out that the ∼0.3 Å movement of iron caused by ligand binding to the heme is communicated to the N-terminus (Trp7) of globin through the proximal His (*33*). Here, we report detailed behaviors of Trp7 and Trp14 in the earlier folding process of apoMb unraveled by the 244 nm excited kinetic UVRR spectra and provide a direct evidence for rapid incorporation of Trp14 into α-helix in the earliest stage of folding.

EXPERIMENTAL PROCEDURES

Materials. ApoMbs were prepared from horse Mb (Sigma, skeletal muscle) and sperm whale Mb (Biozyme) by the 2-methyl ethyl ketone (2-butanone, Nacalai Technology) extraction method of heme (*34*). The protein concentration of the sample was made 60 μM for stationary measurements, and its pH was adjusted by adding a proper amount of 1 M HCl. To avoid possible salt effects such as aggregation and stabilization of an intermediate, buffer was not used in this experiment, and therefore, pH values were checked before and after the UVRR measurements.

A model peptide of the A helix (A peptide), which is slightly modified from the sequence of native the A helix in swMb to raise the solubility and has the sequence NH_2-SEAEAQQAEHAWAKVEADG-COOH, was purchased from Sawady Technology (Tokyo, Japan). The purity of the model peptide, examined by HPLC, was higher than 95%. The A peptide or free tryptophan for reference was dissolved in 50 mM Tris buffer at pH 8, and its concentration of the stock solution was adjusted to 2.4 mM by assuming the molar absorbance of the Trp residue at 280 nm (ϵ_{280}) to be 5690 M^{-1} cm^{-1} (*35*).

UVRR Measurements. UVRR spectra were obtained with 244 nm excitation using an intracavity frequency-doubled CW Ar^+ ion laser (Coherent, Innova FreD). Raman scattered light was collected with a microscope objective lens at 90° geometry, dispersed with a 126 cm single spectrometer (Spex, 1269) equipped with a 3600 grooves/mm holographic grating, and detected with an intensified charge-coupled device (Princeton Instruments, ICCD-1024MG-E/1) (*36*). The laser power at the sample point was less than 200 μW to avoid possible photodegradation. For the equilibrium intermediates, the sample solution at a given pH was put into a spinning cell with a small stirring bar (600 rpm), and UVRR spectra were recorded at 20 °C with the total exposure time of 120 min, although the sample was exchanged with a fresh one every 10 min. Different sensitivities among individual elements of an array detector were corrected by dividing all the observed spectra with the white light spectrum of the D_2 lamp. The spectra were normalized with the water band at 1650 cm^{-1}, and afterward, the water contribution was subtracted from the observed spectra.

Construction and Performance Test of a Rapid Mixing Device. A rapid mixing continuous flow apparatus, which is essentially the same as that reported by Takahashi et al. (*19*), was constructed in this study to observe UVRR spectra of the sub-millisecond kinetic folding intermediates. The mixing ability of this apparatus was examined by the protonation reaction of imidazole (Im) to imidazolium (ImH^+) ion, in which a 100 mM Im solution was mixed with 100 mM citric acid under conditions similar to those used for the measurements of apoMb. The protein concentration in the sample solution for the kinetic pH-jump experiments was made 120 μM with 10 mM HCl at pH 2.2, and it was mixed with the same volume of 100 mM potassium phosphate buffer at pH 6.2 to achieve a pH jump to 5.6.

For the kinetic measurements, the laser power of the 244 nm line was made 120 μW at the sample point, and the delay time of the measurement after mixing of the solution was changed by shifting the observation point along the flow direction. To avoid adhesion of a protein on the cell wall due to UV illumination, the duration time of UV illumination at a given spot on one time was made short by the shifting program of the observation point. One set of delay times (corresponding distances from the mixing point) was initially settled; Raman spectra were accumulated for 2 min at one time at a given observation point, and then the observation point was moved to the next position. After completion of all the presettled delay times, the laser illumination spot was returned to the first observation point and the same measurements were carried out. This cycle was repeated several times, and the spectra for each observation point were digitally added.

Measurements of CD Spectra. CD spectra were measured at 20 °C by using a Jasco J-720WI spectropolarimeter. The concentration of the A peptide was adjusted to 70 μM for various solvent conditions. The helix content was calculated from the mean residue ellipticity at 222 nm using the method of Chen et al. (*37*).

RESULTS

UV RR Spectra of HoloMb and ApoMb. Figure 1 compares the 244 nm excited UVRR spectra of horse holoMb (A) and

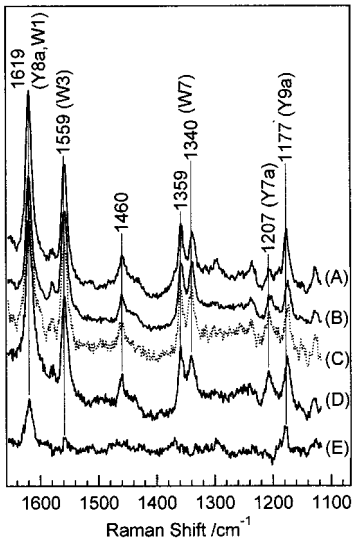

FIGURE 1: The 244 nm excited UVRR spectra of horse holoMb (A) and apoMb (B) at 20 °C in 50 mM phosphate buffer (pH 7.5) containing 100 mM $(NH_4)_2SO_4$ and horse apoMb (C) and sperm whale apoMb (D) under no-salt conditions at pH ~5.3. The concentraton of Mb is 400, 400, 100, and 120 μM for spectra A−D, respectively. Spectrum E represents the difference of spectrum A subtracted from spectrum B by normalizing the two spectra with the band of SO_4^{2-} ions at 980 cm^{-1} (not shown).

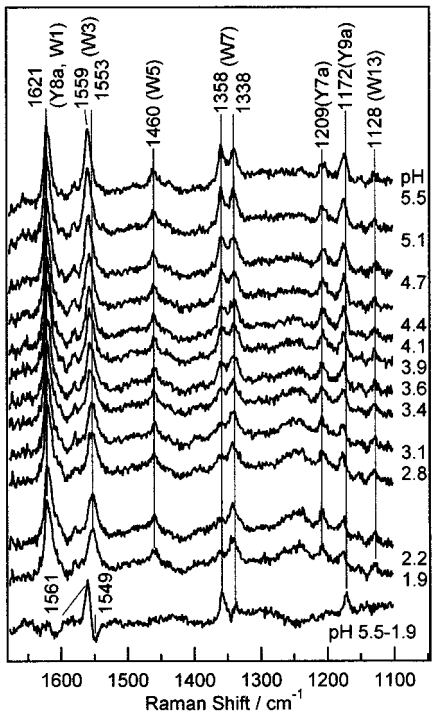

FIGURE 2: Stationary state UVRR spectra of 60 μM horse apoMb at various pH values at 20 °C. The apoMb solutions at various pH values were prepared with a suitable amount of 1 M HCl from the same stock solution. The spectra were normalized with the water band at 1650 cm^{-1}, and the water contribution was subtracted from the observed spectra.

horse apoMb (B) both in buffer at 20 °C and horse apoMb (C) and sperm whale apoMb (D) both under no-salt conditions at pH ~5.3. Since both spectra A and B contain the same amount of SO_4^{2-} ions, which give rise to a Raman band at 980 cm^{-1} (outside of the displayed region), the spectral intensities are normalized with the 980 cm^{-1} band, and their difference was calculated. Spectrum E represents the holo-minus-apo difference. Since the F helix is melted in apoMb, Tyr146, which is hydrogen bonded to the F helix in holoMb, is not held by it, probably being exposed in apoMb. Such a structural difference yields an appreciable difference in the Raman spectrum of Tyr146 between holoMb and apoMb. Since there is no internal standard of intensity for the no-salt spectrum, it is difficult to extract an effect of buffer, but spectrum C is close to spectrum B, indicating that a protein structure is influenced little by the absence of salt. The RR spectrum remained unchanged between pH 5.3 and 7.5 and in the protein concentration range between 100 and 400 μM. The RR spectrum of sperm whale apoMb (spectrum D) is slightly different from that of horse apoMb (spectrum C), and it will be discussed later.

Equilibrium Acid Unfolding. The UVRR spectra of horse apoMb for the equilibrium acid unfolding process at 20 °C are shown in Figure 2, where the trace at the bottom depicts the difference spectrum between pH 5.5 and 1.9, which are termed the native and the acid-unfolded (low salt concentration) states, respectively. In the spectra, the bands arising from Trp and Tyr residues are marked by W and Y, respectively, and the mode numbers according to Harada and Takeuchi (*38*) follow the characters. The difference spectrum indicates that the bands at 1559 (W3), 1358 (W7), and 1172 cm^{-1} (Y9a) decrease in intensity upon acid unfolding. The spectral changes associated with Trp bands are qualitatively in agreement with the reported results obtained from the analysis of the W16 band (*16*). It is noted that the intensity of the 1172 cm^{-1} (Y9a) band of Tyr is already reduced in the spectrum of native apoMb compared with that of holoMb due to removal of a heme group, as pointed out for Figure 1, and further decreases at pH 1.9. The intensity reduction means that the environments of Tyr residues become more hydrophilic, and thus that Tyr side chains are more exposed to solvent in apoMb than in holoMb at pH 5.5, and also more exposed at pH 1.9 than at pH 5.5 (*33*).

The W7 band of the Trp residue (N_1-C_8 stretch) splits into two bands at 1358 and 1338 cm^{-1} due to Fermi resonance with two combination bands (*39*), and their intensity ratio, R ($=I_{1358}/I_{1338}$), is known to be sensitive to the polar and/or nonpolar environments around Trp residues (*38*). The R value of the Trp residue placed under complete exposure to water was 0.48 upon excitation at 244 nm, while the R values of holoMb and apoMb at pH 7 were 1.2 and 1.05, respectively. Since two Trp residues are contained in the A helix and interact with the E−F loop as well as with the H helix (Trp7) or the E, H, and G helices (Trp14), the melting of the F helix may induce appreciable fluctuation in the E−F loop and thus in the environment of Trp.

The W3 band (C_2-C_3 stretch) (*38*) is shifted to lower frequencies and exhibits broadening at lower pH. This feature is expanded in Figure 3a, where solid lines represent the observed spectra. It is known that the W3 frequencies of Trp have a correlation with the torsion angle ($\chi^{2,1}$) of the $C_\alpha-C_\beta-C_3-C_2$ linkage (*40*). The W3 frequency at pH 1.9 is identical with that of tryptophan in an aqueous solution, indicating that the Trp residues of acid-unfolded Mb at pH 1.9 experience no steric hindrance from other parts of the protein.

The frequency shift and intensity decrease of the W3 band with pH could not be satisfactorily interpreted by any

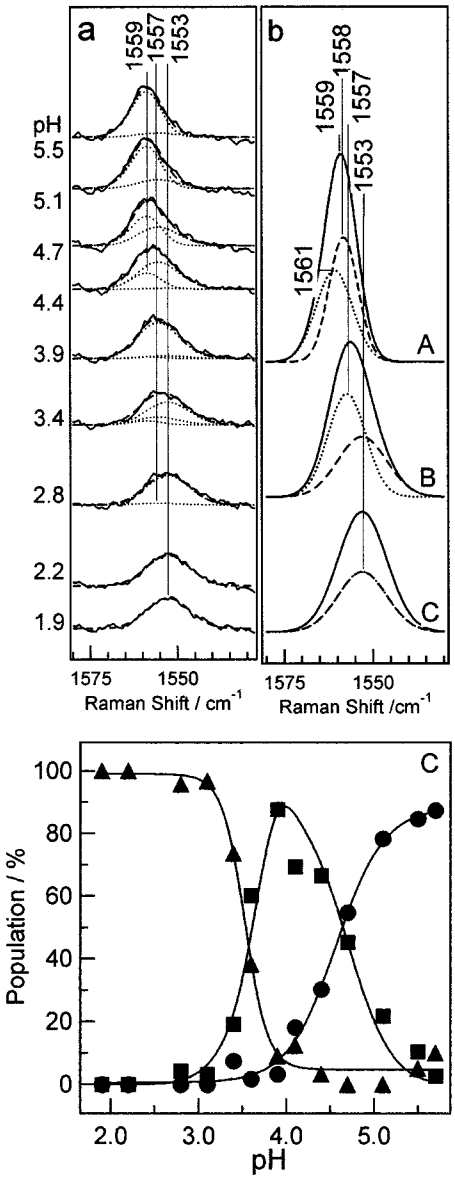

FIGURE 3: (a) Expanded W3 bands of horse apoMb in an equilibrium at various pH values. The solid lines represent the observed spectra, and the dotted lines represent the assumed from the pure native (b-A), intermediate (b-B), and unfolded species (b-C), which have band centers at 1559, 1557, and 1553 cm^{-1}, respectively. The dashed lines represent the simulated spectra (weighted sum of the three assumed spectra). (b) Assumed W3 bands of Trp7 (broken line), Trp14 (dotted line), and the sum of the two Trp spectra for the native (A), intermediate (B), and unfolded states (C). (c) pH dependence of the populations of the native (N, ●), intermediate (I, ▲), and unfolded species (U, ■) calculated from the W3 band. The midpoint pH values for the N ↔ I and I ↔ U transitions are pH 4.5 and 3.5, respectively.

weighted sum of the native and unfolded spectra. Deviation of the observed spectra from the calculated ones, which were simulated under the assumption of the presence of two components, was conspicuous around pH 4, suggesting the spectroscopic appearance of an intermediate around pH 4. Therefore, we tried to simulate the observed spectra with three components, that is, the native, an intermediate, and the unfolded species, according to the following idea. We know from the previous mutation study (*33*) that Trp7 and Trp14 in the native state give the W3 bands at 1558 and 1561 cm^{-1}, respectively. Accordingly, the relative intensity and frequencies observed there, which are illustrated by broken and dotted lines of trace A in Figure 3b, were used as those of native species in the simulation. Both Trp7 and Trp14 in the unfolded state are considered to have the same band shape and intensity as those of an aqueous tryptophan solution, and accordingly, individual Trp residues bear the half-intensity of the observed W3 band at pH 1.9, which is illustrated by a broken line of trace C in Figure 3b.

In the intermediate species, we assumed that Trp7 is already exposed to the protein surface, because the studies on pH dependence of far-UV CD spectra indicated that the A helix of horse apoMb at pH 4 was partially unfolded, while the A helix of sperm whale apoMb almost remained at pH 4 (*20*, *25*). In addition, the previous 229 nm excited UVRR study by Chi and Asher pointed out from the intensity change of the W16 band that Trp7 was exposed at pH 4 in horse apoMb (*16*). Accordingly, it would be reasonable to assume that Trp7 in the intermediate species has a W3 band at 1553 cm^{-1} with the same intensity as that of tryptophan in an aqueous solution, which is illustrated by a broken line of trace B in Figure 3b. Thus, only a spectrum of Trp14 in the intermediate species is unknown. The spectral fitting suggested its presence at 1557 cm^{-1} as depicted by the dotted line of trace B in Figure 3b. In this way, the W3 spectra of Trp7 and Trp14 in the native, intermediate, and unfolded species were determined, and their sum weighted with populations was calculated as shown by the broken lines in Figure 3a, which reproduce well the observed spectra shown by the solid lines. It is noted that since the intensity of the W3 band decreases because of the removal of heme, the calculation of the native state of apoMb using the W3 band of holoMb of two Trp mutants does not allow the component of the native species to reach 100% at pH 5.5.

Figure 3c shows the pH dependence of the population of the three species obtained from spectral fitting of the W3 band displayed in Figure 3a. The population of the native species decreases upon lowering the pH from 5.5 to 4.0, and conversely, the population of the intermediate species increases with the midpoint pH of transition at pH 4.5. Since this intermediate species was a dominant component around pH 4, this will be called the "equilibrium pH 4 intermediate" hereafter. Below pH 4, there are practically two species in equilibrium, that is, the pH 4 intermediate and the unfolded species, with the midpoint pH of transition at ~3.5. This pH value appears to be close to the melting pH of the A helix reported by Chi and Asher (*16*) and that from the phase diagram for acid unfolding of apoMb by Goto and Fink (*41*).

The pH dependence of the *R* value is illustrated in Figure 4, where the values for sperm whale (○) and horse Mbs (●) are shown and the corresponding relative hydrophobicity, which is scaled under the assumption of 100% hydrophobicity for horse holoMb and 0% for the acid-unfolded state, is graduated at the right axis. The *R* value of the native state was 1.05 for horse apoMb (1.2 for holoMb), meaning that the Trp residues were buried in fairly hydrophobic environments in the native apoMb. Since the W7 bands at various pH values could be well fitted by the weighted sum of the native and unfolded spectra, there would be no other effects that determine the relative intensity of the W7 doublet except for hydrophobicity. The plot in Figure 4 indicates the presence of two transitions with midpoint pH values of 4.5 and 3.5, which happen to be identical with the transition pH

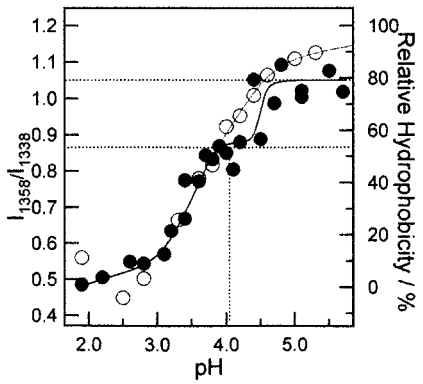

FIGURE 4: pH dependence of the intensity ratio of the W7 doublet ($R = I_{1358}/I_{1338}$) for horse (●) and sperm whale (○) apoMbs (60 μM) at 20 °C. The right axis denotes the degree of relative hydrophobicity, which was scaled by assuming that the R values of holoMb at pH 7 and of apoMb at pH 1.9 are 100 and 0%, respectively. The R values of native apoMb and the equilibrium pH 4 intermediate are 1.05 and 0.85, respectively, meaning that hydrophobicity around Trp for the native apoMb and the pH 4 intermediate is decreased by 20 and 45% compared to that of the native holoMb, respectively.

value for the transition between the native and equilibrium pH 4 intermediate states and that for the transition between the equilibrium pH 4 intermediate and the unfolded states, respectively, which were determined with the W3 band (Figure 3c).

The R value of the equilibrium pH 4 intermediate indicates that the average hydrophobicity in the environments of Trp is 55% of that in the native holoMb. This value is consistent with the calculation based on the idea that Trp7 is fully exposed.[2] Accordingly, it is highly likely that the change from the native to the pH 4 intermediate is accompanied by complete exposure of Trp7 under retention of Trp14 in the hydrophobic environments. This suggests that not only the AGH hydrophobic core but also the E helix are retained in the hydrophobic condensation around the side chain of Trp14, although the hydrogen exchange experiments with NMR indicated that the amide proton of the E helix was not protected from access of solvent water (*20*).

Kinetic Intermediates following the pH Jump. A new rapid mixing apparatus with a dead time much shorter than that of an ordinary one was constructed by Takahashi et al. and successfully applied to a pH-jump folding experiment of cytochrome *c* (*19*). We constructed a similar rapid mixing device combined with a UVRR spectroscopic instrument in this study. The mixing efficiency was examined with the Raman spectral change caused by protonation of imidazole (Im) to imidazolium (ImH^+). Figure 5 shows the UVRR spectra of Im (spectrum A) and ImH^+ (spectrum G) under the equilibrium conditions and kinetic spectra of Im upon mixing with 100 mM citric acid flowing at various flow rates (spectra B−F). The Raman bands of Im at 1258 and 1327 cm^{-1} are definitely distinguished from those of ImH^+ at 1213 and 1458 cm^{-1}. It was confirmed empirically that the resonance enhancement effect of intensity on Im bands upon excitation at 244 nm makes it possible to detect the remaining Im as small as 3%.

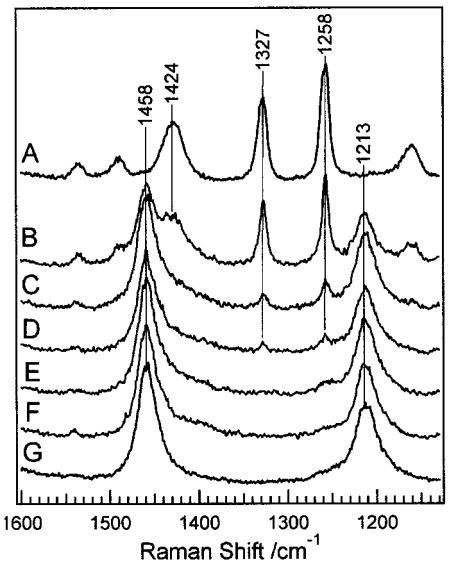

FIGURE 5: UVRR spectra of imidazole (A) and imidazolium ion (G) and kinetic spectra (B−F) observed at 450 μm apart from the mixing plate in which a neutral imidazole solution is mixed with citric acid for the pH jump. The flow rate and the time required for moving from the mixing point to the observation point are as follows: (B) 1.5 mL/min and 900 μs, (C) 2.5 mL/min and 540 μs, (D) 3 mL/min and 450 μs, (E) 6 mL/min and 225 μs, and (F) 9 mL/min and 150 μs. The mixing efficiency and dead time significantly depend on the flow rate.

When Im is mixed with citric acid, the UVRR bands of ImH^+ appeared at 1458 and 1213 cm^{-1}, and simultaneously, the two strongest Im bands at 1258 and 1327 cm^{-1} became weaker. Kinetic spectra B−F were observed at the point which is 450 μm apart from the mixing point for various flow rates (1.5, 2.5, 3.0, 6.0, and 9.0 mL/min, respectively),[3] and thus reflected the spectra for delay times of 900, 560, 450, 225, and 150 μs after mixing, respectively. The Raman calibration curve determined separately under the same excitation conditions indicates that the percentages of the remaining Im in spectra B−F are 60, 15, 10, 3, and 0%, respectively. The results mean that the efficiency of mixing depends on the flow rate, and mixing is complete 150 μs after mixing under the flow rate of 9.0 mL/min. Thus, the mixing time was proven to be faster than 150 μs under this flow rate. This flow rate was adopted in the following pH-jump experiment of apoMb from pH 2.2 to 5.6, and the delay time after mixing was changed by moving the observation point along the flow direction.

Typical spectra observed in the kinetic measurements are shown in Figure 6, where the spectra for the stationary states at pH 2.2 and 5.6 are presented at the bottom and top, respectively. The Trp W3 band at 1553 cm^{-1} in the acidic solution is shifted to 1559 cm^{-1} and sharpened in the neutral solution, and the relative intensity of the W7 doublet ($R = I_{1358}/I_{1338}$) is also changed. This feature is well-reproduced by the stationary spectrum of the mixture of the unfolded

[2] In the previous study of the W7F and W14F mutants of Mb, we concluded that the environment of Trp14 was 1.3 times more hydrophobic than that of Trp7 (*33*). If a parameter representing the extent of Trp7 that is buried is X, the corresponding parameter of Trp14 would be 1.3X, and their average (2.3X/2) corresponds to the experimental hydrophobicity of Trp in the native holoMb. When Trp7 is exposed completely ($X = 0$) at pH 4 while Trp14 remains buried, the average value of the buried parameter is 1.3X/2, and it would correspond to 57% hydrophobicity [(1.3X/2)/(2.3X/2)] of the native holoMb, in agreement with the observed value.

[3] These flow rates correspond to flow speeds of 0.5, 0.83, 1.0, 2.0, and 3.0 m/s.

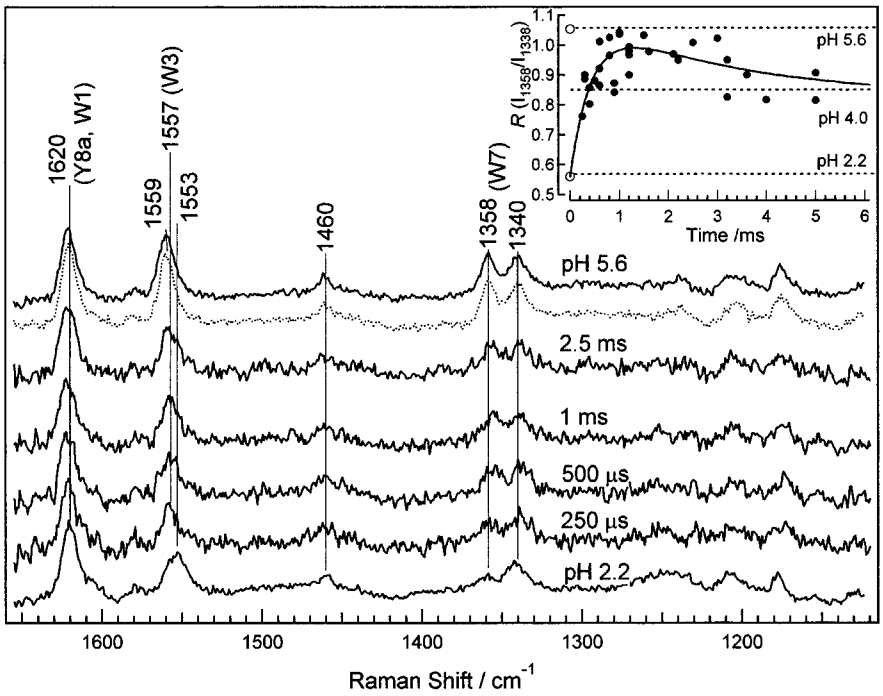

FIGURE 6: Time-resolved UVRR spectra excited by the 244 nm CW laser following the pH jump from 2.2 to 5.6 at 20 °C. The top and bottom traces represent the stationary state spectra obtained at pH 5.6 and 2.2, respectively. The spectrum represented by the dotted line shows the spectrum of the stationary mixture of the unfolded sample with the refolding buffer. Delay times of the observation after the mixing of two solutions by the rapid mixing device are specified on each spectrum. The inset shows the time dependence of the observed *R* values (●). The *R* values of the unfolded state at pH 2.2 ($R = 0.56$) and the native state ($R = 1.05$) are also included at time zero (○). The solid line denotes the theoretical results calculated under the assumption that two successive first-order reactions ($I_1 \rightarrow I_2 \rightarrow I_3$) occur to change the *R* value: $\tau_1 = 0.4$ ms and $\tau_2 = 3$ ms.

sample with the refolding buffer depicted with a dotted line. The relative intensity of the W7 doublet suggested that the environment of Trp is still hydrophilic 250 μs after the pH jump but has been changed at 1 ms. The inset shows the time profile of the *R* value.

It is noted from this plot that the *R* value becomes maximum around 1 ms but decreases slowly around 2−5 ms. Fitting of the *R* value changes with the model of two successive first-order reactions ($I_1 \rightarrow I_2 \rightarrow I_3$), which is represented by the solid line in the inset, yielded the following rate constants: $k_{1,2} = 2.5 \times 10^3$ s^{-1} and $k_{2,3} = 0.33 \times 10^3$ s^{-1} (which correspond to $\tau_1 = 0.4$ ms and $\tau_2 = 3$ ms, respectively). Here I_1 is not always the same as the unfolded state (U) as will be discussed later. The *R* value was 1.05 for I_2 and 0.83 for I_3. The value for I_3 is the same as that obtained for the equilibrium pH 4 intermediate. The value of 1.05 for I_2 is close to that of the native state, and therefore, the contribution of a single Trp14 residue cannot account for the value of 1.05, if Trp7 is left exposed in the hydrophilic environments. It is suggested as its consequence that the environment of Trp7 once becomes hydrophobic (buried in the folded part) in I_2 and returns to being somewhat hydrophilic (exposed to solvent) in I_3. It may mean that Trp7 is involved in the "hydrophobic condensation" in the $I_1 \rightarrow I_2$ process and also in the "hydrophobic rearrangements" in the $I_2 \rightarrow I_3$ process. Note that such features have not been recognized in the absence of time-resolved UVRR experiments and that the spectra for the equilibrium unfolding process are apt to allow a transient species with a short lifetime to pass unnoticed.

It was confirmed with the expanded spectra (not shown) of the W3 region of the time-resolved UVRR spectra of Figure 6 that a frequency of the W3 band is already shifted from 1553 to 1557 cm^{-1} in the earliest delay time observed after the pH jump (0.25 ms), at which the W7 doublet exhibits only a little change. This fact means that the structural change on the $\chi^{2,1}$ angle ($C_2-C_3-C_\beta-C_\alpha$ torsion angle of the Trp side chain) occurs prior to the environmental change and yields the first intermediate (I_1), that is, before 0.25 ms, while Trp residues are still left in the hydrophilic environments. It will be demonstrated below that this frequency shift of the W3 band is caused by incorporation of Trp14 into the α-helix. The frequency of 1557 cm^{-1} remains unchanged between 0.4 and 3.2 ms and is the same as that observed for the equilibrium pH 4 intermediate.

The frequency change of the W3 band from 1557 to 1559 cm^{-1}, the frequency of the native state (N), did not occur even 40 ms after the pH jump, which was the longest allowable delay time with the present apparatus. This means that the conversion from the last intermediate (I_3) to the native state must be a very slow process. Other studies also reported that the conversion of the last intermediate to the native state takes on the order of seconds (*21*). While the side chain of Trp14 is already fixed in a certain structure in the I_1 state, the final arrangement of the $\chi^{2,1}$ angle (from 1557 to 1559 cm^{-1}) would take place in the rate-limiting step ($I_3 \rightarrow$ N) of the whole folding reaction.

Measurements of CD and UVRR Spectra of the A Peptide. To examine the effect of secondary structure formation on the W3 band, we prepared a model peptide of the A helix of Mb (A peptide) as described in Experimental Procedures. The sequence of the model peptide was based on that of the A helix in swMb, since the helical propensity of the A helix of swMb is higher than that of hMb (*25*). We changed a

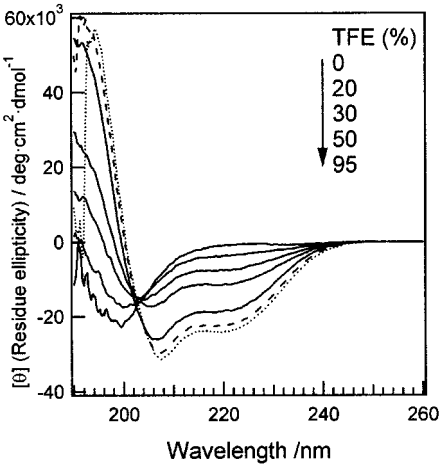

FIGURE 7: CD spectra of the A peptide observed for various mixed solvents: varied concentrations of TFE in water (solid lines), 95% methanol (dotted line), and a mixture of 42.5% TFE with 42.5% MeOH (broken line).

few residues to increase the helical propensity and furthermore to increase the solubility, since a peptide with the native sequence of the A helix is hard to dissolve in water (*42*). Thus, Trp7 and other hydrophobic residues, which are located far from Trp14 and are considered to have no interaction with Trp14 on the basis of X-ray structures of Mb, were changed to Ala or Glu. As a result, the prepared model peptide could easily be dissolved in water around pH 8 and enabled us to measure its CD spectra in various solvents at 20 °C. The CD spectra for its water/trifluoroethanol (TFE) mixed solvents (0−95%) are displayed in Figure 7, where spectra for MeOH (42.5%)/TFE (42.5%)/water (15%) (broken line) and MeOH (95%)/water (5%) mixed solvents (dotted line) are also shown. In water (50 mM Tris buffer at pH 8), the A peptide has a random coil structure. Addition of alcohols, such as TFE and methanol (MeOH), increased the negative ellipticity at 207 and 222 nm, an indication of formation of an α-helix. The helix contents calculated by the mean residue ellipticity at 222 nm indicated that the A peptide had ∼50% helical structures in 95% TFE. The helix contents were nearly proportional to the concentration of TFE.

Figure 8 shows the 244 nm excited UV resonance Raman spectra of the A peptide (solid lines) and free Trp (broken lines) in various solvents (A−D). Because of interference from strong Raman bands of TFE and MeOH in the measurement of the peptide and free tryptophan bands, the concentration of TFE was adjusted to 70% (v/v) and that of MeOH to 75% (v/v). The contributions of the solvent bands were subtracted from the observed spectra, and the resultant spectra were roughly normalized with the intensity of the W5 band at 1460 cm^{-1}. The inset shows the expanded spectra of the W3 band region. In water (spectrum A), the W3 bands of the A peptide and free Trp appeared at 1552 cm^{-1}. The W3 band of a free Trp solution was hardly altered by changes in solvent properties except a slight change for the 70% TFE solvent (spectrum B). On the other hand, the W3 bands of the A peptide in solutions with alcohol added were shifted to 1555 cm^{-1} [B for 70% (v/v) TFE, C for 75% MeOH, and D for 32.5% TFE and 32.5% MeOH]. The differences between the peptide and free Trp are obvious in all cases. While the Raman shift of the W3 band in the model peptide

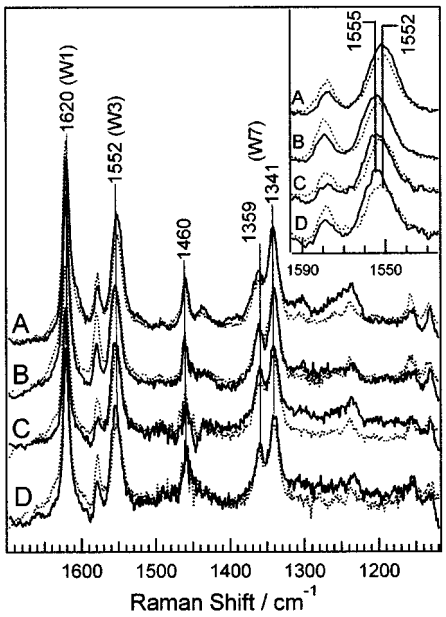

FIGURE 8: The 244 nm excited UVRR spectra of a free tryptophan solution (broken lines) and the A peptide (solid lines) in various solvents both at 600 μM: (A) water, (B) 70% (v/v) TFE, (C) 75% (v/v) MeOH, and (D) 32.5% TFE and 32.5% MeOH. The inset shows the expanded spectra for the W3 band.

upon helix formation is smaller than that in apoMb due to a helix content of only ∼35% in 70−75% alcohol, this observation supports the idea that incorporation of a Trp residue into the α-helix influences the $\chi^{2,1}$ angle and thus the W3 frequency.

The intensity ratio (I_{1358}/I_{1338}) of the W7 doublet (*R* value), which should be sensitive to the polar or nonpolar environment around a Trp side chain (*39*), is slightly higher for the A peptide than for a free amino acid in all the solutions, presumably in a less polar environment in the helix. The *R* value of the A peptide decreased in the following order: 75% MeOH > mixture of MeOH with TFE > 70% TFE > water.

DISCUSSION

Horse and Sperm Whale Mbs. Since the accumulated data for the folding process of apoMb have been derived from both horse (hMb) and sperm whale Mb (swMb) and they are partly controversial, it is important to compare the two Mbs first. Due to the replacement of Tyr151 in swMb with Phe151 in hMb, the intensities of Tyr bands for hMb are two-thirds of those of swMb as shown by spectra C and D in Figure 1. Apart from this, the Trp UVRR bands were similar between hMb and swMb in the native holoMb (*33*), but slightly dissimilar in apoMb, more hydrophobic for sw-apoMb than h-apoMb at pH 5.6. Furthermore, pH dependencies of the W7 doublet of apoMb were different as shown in Figure 4. The pH dependencies of the Raman frequency shift and intensity change of the W3 band were also different between h-apoMb and sw-apoMb. This difference seems to reflect the differences in the helix forming propensity of the A helix.

The α-helix content of the whole protein at pH 4.2 was lower than the sum of the contents of the A, G, and H helices for h-apoMb, whereas it was higher for sw-apoMb (*25*). Furthermore, NMR studies showed that most of the A helix was formed at pH 4 in sw-apoMb (*22*). Since the equilibrium

intermediate species at pH 4 has the AGH helix core, in which the A helix has contacts with the stable G and H helices at the C-terminal side of the A helix, it is reasonable to assume that the N-terminal side of the A helix is more melted in hMb than in swMb, and accordingly, Trp residues might be influenced by it. In the analysis of fluorescence spectra of apoMb (*43*), it is assumed that the fluorescence of Trp14 is more quenched by Met131 of the H helix depending on their distance, but that of Trp7 is not influenced by Met131. However, the discussion about Trp7 requires some caution due to possible differences between hMb and swMb. The results presented here suggest that Trp7 of h-apoMb in the equilibrium pH 4 intermediate is exposed to solvent in the form of random coil, in agreement with Chi and Asher (*16*), while Trp7 of sw-apoMb is considered to stay still on the A helix and in contact with the H helix (*18*).

Structural Characteristics of the Equilibrium pH 4 Intermediate. The structures of Trp residues deduced from the analysis of the W3 and W7 bands in this study are in good agreement with those reported previously by Chi and Asher; that is, Trp7 is fully exposed, and Trp14 is still buried in the hydrophobic core in the pH 4 folding intermediate of horse apoMb. Here, we discuss the structural change of Trp side chains accompanied by the formation of the secondary structure and the tertiary contacts. Although the study of the packing process of the secondary structures is not easy with conventional methods, vibrational spectra of Trp can serve as a direct probe of the structural changes around Trp side chains. The frequency shift of the W3 band between the native and the equilibrium pH 4 intermediate indicates that some steric interaction is present between the A and E helices in the native state but is absent in the pH 4 intermediate. In holoMb, the presence of heme would help the globin overcome the potential barrier of this final step in folding toward construction of the active site. In this regard, the folding process of Mb seems to consist of two independent steps, including the formation of the "frame" structure and the construction of the "functional" site.

The equilibrium unfolding intermediate of apoMb at pH 4 has been studied extensively using various spectroscopic techniques (*20*, *22*, *23*, *25*, *29*, *41*, *44*, *45*). Many of them concluded that the equilibrium pH 4 intermediate was the same as the kinetic intermediate appearing in the millisecond time regime for neutral solutions (*21*, *26*, *28*, *46*, *47*). In this intermediate, the G, H, and A helices are fully or partially folded (*20*, *22*) and the nativelike AGH hydrophobic core is formed (*48*). On the basis of these studies, the structure of native apoMb seems to be categorized into two structural portions, regions I and II. Region I includes the A, G, and H helices, which remain intact in the equilibrium pH 4 intermediate, and constitutes the frame of the globin structure. Accordingly, region I must be formed in the earlier stage of folding and provide a rigid core for construction of region II. Region II includes the B−F helices, which are almost frayed in the equilibrium pH 4 intermediate, and constitutes the functional site. The tertiary structure formation of region II is the rate-limiting step of the folding process. Most residues which control the ligand binding and recognition, including the distal and proximal His, are contained in this region. Two introns which devide the gene of Mb into three parts interpose B and G helices (*49*).

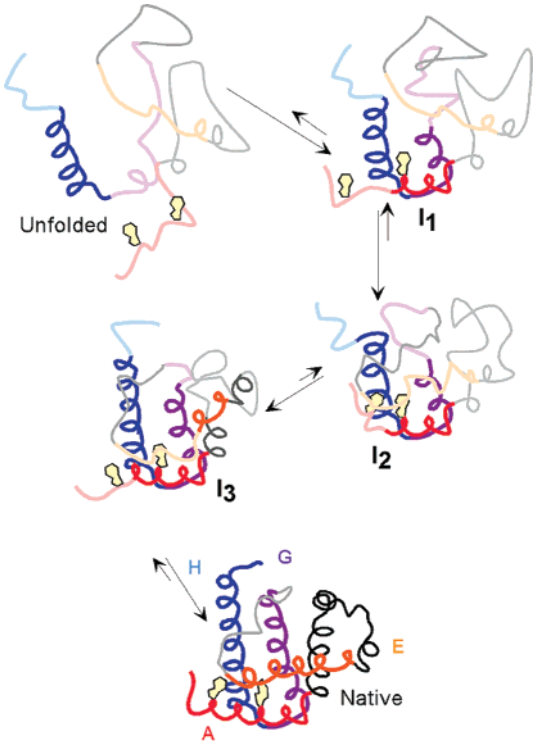

FIGURE 9: Schematic diagram for folding of apoMb derived from the kinetic UVRR experiments described herein. The deep- and light-colored regions indicate that the structure formation is complete and incomplete, respectively. Trp7 and Trp14 are attached to the red segment. I_1 has a local structure for which the frequency of the W3 band is shifted to 1557 cm^{-1} in the dead time of the pH jump. I_2 contains a large hydrophobic core around the AGH helices. The character of I_3 seems to be similar to that of the equilibrium pH 4 intermediate, in which the torsion angle of the Trp indole plane is different from that of the native state.

Many experiments using mutants tried to determine whether the factor stabilizing the equilibrium pH 4 intermediate is the nativelike specific hydrophobic contacts or nonspecific hydrophobic interaction (*48*, *50*, *51*). The Trp14 → Phe mutation had a small effect on the stability of the equilibrium pH 4 intermediate, indicating that Trp14 contributes to the native specific interaction as well as to nonspecific hydrophobic interaction (*51*). The independence of the frequency shift of the W3 band from the increase in the hydrophobicity in the earlier stage of folding ($I_1 \rightarrow I_2$) supports the idea that the Trp14 has nonspecific interaction with the hydrophobic core present in the equilibrium pH 4 intermediate. In contrast, the packing process from the intermediate to the native structure ($I_3 \rightarrow N$), that is, the formation process of the correct native contact between the A and E helices, caused the frequency shift of the W3 band from 1557 to 1559 cm^{-1} (change of the $C_2-C_3-C_\beta-C_\alpha$ torsion angle) under the same hydrophobicity.

What Does Occur in the Earliest Stage of the Folding Event of ApoMb? A view from this study is illustrated in Figure 9. In this experiment, the W3 band had already been shifted in the I_1 intermediate from the value of the unfolded state before the hydrophobic environment was produced. This was demonstrated by the 250 μs spectrum in Figure 6 and attributed to the inclusion of Trp14 into the α-helix. The conclusion was derived from the experiments with a model peptide of the A helix. Although the model peptide had some substitution of amino acid residues from the A helix to

increase the helicity and solubility, the CD measurements confirmed the formation of the α-helix for the A peptide in alcohol-mixed solvents but not in water (Figure 7). The W3 band of Trp was shifted slightly but definitely to higher frequencies in the helix-forming solvents compared with that in water (Figure 8). The W3 frequency of the peptide in water was the same as that of the free tryptophan solution. Consequently, the frequency shift from 1553 to 1557 cm^{-1} in the earliest stage of folding ($U \rightarrow I_1$) is compatible with the secondary structure change of Trp14 from a random coil to the α-helix. Although it is difficult to estimate the correct hydrophobicity around Trp14 in I_1, it is plausible that I_1 corresponds to the E intermediate having some limited contacts among the H, G, and A helices, reported by Callender and co-workers (*30*).

The change in the *R* value (inset of Figure 6) clearly indicated that a state with increased hydrophobicity in the environments of Trp has been generated prior to reaching the equilibrium pH 4 intermediate (I_3). The feature is rather unexpected. This second kinetic intermediate (I_2), which appeared with the formation rate of 2.5×10^3 s^{-1}, has two Trp residues in the hydrophobic environments. Although Trp7 is exposed to solvent in the equilibrium pH 4 intermediate, the environment of Trp7 in I_2 was hydrophobic. Presumably, a large-scale hydrophobic collapse involving Trp7 would have occurred on the random coils, because the core of AGH helices alone cannot keep many hydrophobic side chains without exposing to solvent. It is likely that the hydrophobic side chains on the frayed E and F helices and the N-terminal residues on the frayed A helix gathered around the core of AGH helices, playing a role as a hydrophobic nucleus. In this stage, the helicity would not increase and the backbone could move flexibly. The rate of formation of the A helix and the flexibility of Trp7 might be different between hMb and swMb in this time regime. To form the third intermediate (I_3), which is close to the equilibrium pH 4 intermediate, the A and B helices would be extended and the melted E helix would be located in the topologically right position, while Trp7 is made exposed to the solvent again.

The side chain conformation of Trp, suggested by the 1557 cm^{-1} band of these intermediates, is a consequence of restriction from other parts of the protein, and its release from the restriction allows assembly of the native hydrophobic core ($I_3 \rightarrow N$). The origin of the structural restriction of the Trp side chain might be the local contacts caused by the formation of the α-helix. This view is in agreement with the studies of the fluorescence anisotropy decay kinetics of peptides (*52*) and the NOE measurements of melittin (a peptide) (*53*), which concluded that the mobility of the Trp side chain is more restricted in a helix than in a random coil. There is an argument that the mobility of Trp in the I_3 intermediate of apoMb is more restricted than that in a helixed peptide (*54*). Since the indole ring of Trp14 has contacts with Val17 and Glu18 of the A helix according to X-ray crystallographic data (*55*), there is a possibility that these side chains somewhat restrict movement of Trp14. The fact that the formation of local structure is faster than the increase in hydrophobicity of the environment around the aromatic residues supports the framework model (*56*) emphasized by the diffusion−collision process as pointed out hitherto (*57*, *58*).

The temperature-jump experiment from cold denaturation exhibited very fast fluorescence quenching (2.0×10^5 s^{-1}), and it was considered that the A helix was in the proximity of the G and H helices, that is, rapid formation of the core of AGH helices (*43*, *59*). This is based on the assumption that the changes in fluorescence arise solely from Trp14 through quenching by the approaching Met131 of the H helix. The IR observation of α-helix formation indicated that the rate of formation of the AGH core reached the diffusion limit (1.0×10^4 s^{-1}), although the total helicity was as low as ∼10% (*60*). The time scale of the reaction would depend on the conditions of the system, particularly in the denatured state, because cold denaturation restricts the space and conformation for related residues. It seems likely that local α-helix conformations, which include small hydrophobic patches, diffuse until colliding together and are stabilized by adhesion of three helices termed the AGH hydrophobic core. The presence of another intermediate at low pH is suggested by the fluorescence (*26*, *46*, *61*) and IR spectra (*60*). The characters of these intermediates are not clear except that the A, G, and H helices are partially formed and have contacts with each other. This species may correspond to I_1 of the present kinetic intermediates, although we failed to characterize these intermediates in the equilibrium acid unfolding process.

CONCLUSION

Taking advantage of the sensitive dependence of the W3 frequency on the torsion angle of the Trp indole ring, we succeeded in detecting the structural change of the Trp side chain during the formation ($U \rightarrow I_1$) and rearrangement ($I_3 \rightarrow N$) of helices in apoMb by using UVRR spectroscopy. The mobility of Trp side chains was somewhat restricted in the earlier stage (I_1), though the restriction was different from the interaction in the native state. The change in hydrophobicity around Trp revealed by the intensity ratio of the W7 doublet suggested that the secondary structure was locally formed in the I_1 state prior to hydrophobic collapse. Since the rates of formation of α-helices are different between regions I and II and collisions among α-helices occurred in the first step ($U \rightarrow I_1$) before the formation of the A helix was completed, the folding process of apoMb might be approximately explained by the diffusion−collision model. This is the first direct observation of the structural restriction and environmental changes of a Trp side chain of apoMb in the early stage of folding from the almost unfolded structure.

ACKNOWLEDGMENT

We are grateful to Dr. S. Takahashi of Kyoto University (Kyoto, Japan) for his kind help and advice about the construction of the continuous flow mixing device.

REFERENCES

1. Anfinsen, C. B. (1973) *Science 181*, 223−230.
2. Mitsutake, A., Sugita, Y., and Okamoto, Y. (2001) *Biopolymers 60*, 96−123.
3. Kinoshita, M., Okamoto, Y., and Hirata, F. (2000) *J. Am. Chem. Soc. 122*, 2773−2779.
4. Wolynes, P. G., Onuchic, J. N., and Thirumalai, D. (1995) *Science 267*, 1619−1620.
5. Gilmanshin, R., Williams, S., Callender, R. H., Woodruff, W. H., and Dyer, R. B. (1997) *Biochemistry 36*, 15006−15012.

6. Spiro, T. G. (1988) *Biological Application of Raman Spectroscopy*, Vol. 3, John Wiley and Sons, New York.
7. Mizutani, Y., and Kitagawa, T. (2001) *Chem. Rec. 1*, 258−275.
8. Kitagawa, T., and Ogura, T. (1997) *Prog. Inorg. Chem. 45*, 431−479.
9. Kitagawa, T. (1992) *Prog. Biophys. Mol. Biol. 58*, 1−18.
10. Peterson, E. S., and Friedman, J. M. (1998) *Biochemistry 37*, 4346−4357.
11. Nagai, M., Wajcman, H., Lahary, A., Nakatsukasa, T., Nagatomo, S., and Kitagawa, T. (1999) *Biochemistry 38*, 1243−1251.
12. Nagatomo, S., Nagai, M., Tsuneshige, A., Yonetani, T., and Kitagawa, T. (1999) *Biochemistry 38*, 9659−9666.
13. Hu, X., Rodgers, K. R., Mukerji, I., and Spiro, T. G. (1999) *Biochemistry 38*, 3462−3467.
14. Copeland, R. A., and Spiro, T. G. (1985) *Biochemistry 24*, 4960−4968.
15. Chi, Z., and Asher, S. A. (1998) *Biochemistry 37*, 2865−2872.
16. Chi, Z., and Asher, S. A. (1999) *Biochemistry 38*, 8196−8203.
17. Lednev, I. K., Karnoup, A. S., Sparrow, M. C., and Asher, S. A. (1999) *J. Am. Chem. Soc. 121*, 4076−4077.
18. Hashimoto, S., Fukasaka, J., and Takeuchi, H. (2001) *J. Raman Spectrosc. 32*, 557−563.
19. Takahashi, S., Yeh, S. R., Das, T. K., Chan, C. K., Gottfried, D. S., and Rousseau, D. L. (1997) *Nat. Struct. Biol. 4*, 44−50.
20. Hughson, F. M., Wright, P. E., and Baldwin, R. L. (1990) *Science 249*, 1544−1548.
21. Jennings, P. A., and Wright, P. E. (1993) *Science 262*, 892−896.
22. Eliezer, D., Yao, J., Dyson, H. J., and Wright, P. E. (1998) *Nat. Struct. Biol. 5*, 148−155.
23. Griko, Y. V., Privalov, P. L., Venyaminov, S. Y., and Kutyshenko, V. P. (1988) *J. Mol. Biol. 202*, 127−138.
24. Goto, Y., Takahashi, N., and Fink, A. L. (1990) *Biochemistry 29*, 3480−3488.
25. Sabelko, J., Ervin, J., and Gruebele, M. (1998) *J. Phys. Chem. B 102*, 1806−1819.
26. Jamin, M., and Baldwin, R. L. (1998) *J. Mol. Biol. 276*, 491−504.
27. Luo, Y., and Baldwin, R. L. (2001) *Biochemistry 40*, 5283−5289.
28. Eliezer, D., Jennings, P. A., Wright, P. E., Doniach, S., Hodgson, K. O., and Tsuruta, H. (1995) *Science 270*, 487−488.
29. Kataoka, M., Nishii, I., Fujisawa, T., Ueki, T., Tokunaga, F., and Goto, Y. (1995) *J. Mol. Biol. 249*, 215−228.
30. Gilmanshin, R., Gulotta, M., Dyer, R. B., and Callender, R. H. (2001) *Biochemistry 40*, 5127−5136.
31. Eliezer, D., and Wright, P. E. (1996) *J. Mol. Biol. 263*, 531−538.
32. Lecomte, J. T., Kao, Y. H., and Cocco, M. J. (1996) *Proteins 25*, 267−285.
33. Haruta, N., Aki, M., Ozaki, S., Watanabe, Y., and Kitagawa, T. (2001) *Biochemistry 40*, 6956−6963.
34. Teale, F. W. (1959) *Biochim. Biophys. Acta 35*, 543.
35. Edelhoch, H. (1967) *Biochemistry 6*, 1948−1954.
36. Aki, M., Ogura, T., Shinzawa-Itoh, K., Yoshikawa, S., and Kitagawa, T. (2000) *J. Phys. Chem. B 104*, 10765−10774.
37. Chen, Y. H., Yang, J. T., and Martinez, H. M. (1972) *Biochemistry 11*, 4120−4131.
38. Harada, I., and Takeuchi, H. (1986) *Adv. Spectrosc.*, 113−175.
39. Harada, I., Miura, T., and Takeuchi, H. (1986) *Spectrochim. Acta 42a*, 307−312.
40. Miura, T., Takeuchi, H., and Harada, I. (1989) *J. Raman Spectrosc. 20*, 667−671.
41. Goto, Y., and Fink, A. L. (1990) *J. Mol. Biol. 214*, 803−805.
42. Reymond, M. T., Merutka, G., Dyson, H. J., and Wright, P. E. (1997) *Protein Sci. 6*, 706−716.
43. Ballew, R. M., Sabelko, J., and Gruebele, M. (1996) *Nat. Struct. Biol. 3*, 923−926.
44. Griko, Y. V., and Privalov, P. L. (1994) *J. Mol. Biol. 235*, 1318−1325.
45. Loh, S. N., Kay, M. S., and Baldwin, R. L. (1995) *Proc. Natl. Acad. Sci. U.S.A. 92*, 5446−5450.
46. Jamin, M., and Baldwin, R. L. (1999) *J. Mol. Biol. 292*, 731−740.
47. Tsui, V., Garcia, C., Cavagnero, S., Siuzdak, G., Dyson, H. J., and Wright, P. E. (1999) *Protein Sci. 8*, 45−49.
48. Kay, M. S., Ramos, C. H., and Baldwin, R. L. (1999) *Proc. Natl. Acad. Sci. U.S.A. 96*, 2007−2012.
49. Go, M. (1985) *Adv. Biophys. 19*, 91−131.
50. Hughson, F. M., Barrick, D., and Baldwin, R. L. (1991) *Biochemistry 30*, 4113−4118.
51. Kay, M. S., and Baldwin, R. L. (1996) *Nat. Struct. Biol. 3*, 439−445.
52. Semisotnov, G. V., Zikherman, K. K., Kasatkin, S. B., Ptitsyn, O. B., and Anufrieva, E. V. (1981) *Biopolymers 20*, 2287−2309.
53. Kemple, M. D., Buckley, P., Yuan, P., and Prendergast, F. G. (1997) *Biochemistry 36*, 1678−1688.
54. Tcherkasskaya, O., Ptitsyn, O. B., and Knutson, J. R. (2000) *Biochemistry 39*, 1879−1889.
55. Evans, S. V., and Brayer, G. D. (1990) *J. Mol. Biol. 213*, 885−897.
56. Kim, P. S., and Baldwin, R. L. (1990) *Annu. Rev. Biochem. 59*, 631−660.
57. Bashford, D., Cohen, F. E., Karplus, M., Kuntz, I. D., and Weaver, D. L. (1988) *Proteins 4*, 211−227.
58. Karplus, M., and Weaver, D. L. (1994) *Protein Sci. 3*, 650−668.
59. Ballew, R. M., Sabelko, J., and Gruebele, M. (1996) *Proc. Natl. Acad. Sci. U.S.A. 93*, 5759−5764.
60. Gilmanshin, R., Callender, R. H., and Dyer, R. B. (1998) *Nat. Struct. Biol. 5*, 363−365.
61. Gilmanshin, R., Dyer, R. B., and Callender, R. H. (1997) *Protein Sci. 6*, 2134−2142.

BI012027G